Nanomed. J. 10(4): 313-322, Autumn 2023

RESEARCH PAPER

Investigation and comparison of laser and ultrasound effects on the temperature increasing of the solutions containing graphene oxide nanoparticles for thermal treatment of osteosarcoma cancer cells

Najmeh Sadat Hosseini Motlagh [1*], Elyas Sharifi [2], Bibi Fatemeh Ghiralsadat [3], Mohsen Sardari Zarchi [4], Fatemeh Yaghoubi [5], Fatemeh Oroojalian [6,7*]

[1]Department of Biomedical Engineering, Meybod University, PO Box 89616-99557, Meybod, Iran
[2]Department of Biology, Taft Payame Noor University, Yazd, Iran
[3]Department of Advanced Medical Sciences and Technologies, School of Paramedicine, Shahid Sadoughi University of Medical Sciences, Yazd, Iran
[4]Department of Computer Engineering, Meybod University, Meybod, Iran
[5]Department of Nursing, Shirvan Faculty of Nursing, North Khorasan University of Medical Sciences, Bojnūrd, Iran
[6]Department of Advanced Technologies, School of Medicine, North Khorasan University of Medical Sciences, Bojnūrd, Iran
[7]Natural Products and Medicinal Plants Research Center, North Khorasan University of Medical Sciences, Bojnūrd, Iran

ABSTRACT

Objective(s): The waves of ultrasound and laser in the presence of nanoparticles are introduced as desirable candidates for the thermal treatment of cancer due to having fewer side effects, more speed, and superior treatment efficiency. Here, 2D Graphene oxide nanoparticle is used as a thermal nano-convertor for increasing the yield of thermal cancer therapy.

Materials and Methods: The temperature of GO (in 0.2 and 0.4 mg/ml concentrations) and deionized water regarding heater, bath sonicate, probe sonicate (at a power range of 2-3.5 W), and laser properties at 808 nm with continuous wave (at a power of 0-2 W) in 10 min are investigated. Based on the experimental results, the effect of laser and ultrasound radiation on the temperature is simulated using a data mining approach.

Results: Experimental and simulation results show that GO nanoparticle in this form is unsuitable for converting ultrasound waves into heat. But it is a strong absorber for electromagnetic waves at 808 nm and can raise the temperature to 85 °C. The results indicate that the laser + GO enhances the mortality percentage and treatment yield of MG63 cancerous cells by up to 85%. Also, GO uptake is analyzed by fluorescent microscopic images.

Conclusion: This analysis confirmed that GO is important when laser radiation is used but not when Ultrasound is employed. Also, GO is an excellent photothermal nanoparticle for localized thermal therapy of osteosarcoma cancer cells by laser at 808 nm with low side effects.

Keywords: *Cancer, Graphene oxide, Laser, Thermal therapy, Ultrasound*

How to cite this article
Hosseini Motlagh NS, Sharifi E, Ghiralsadat BF, Sardari Zarchi M, Yaghoubi F, Oroojalian F. investigation and comparison of laser and ultrasound effects on the temperature increasing of the solutions containing graphene oxide nanoparticles for thermal treatment of osteosarcoma cancer cells. Nanomed J. 2023; 10(4): 313-322. DOI: 10.22038/NMJ.2023.74019.1802

INTRODUCTION

Osteosarcoma is the most common primary cancer tumor of the bone, which is more common among children and young people. Unfortunately, current treatments for osteosarcoma often are not effective enough. Multiple drug resistance related to the toxicity of therapeutics in osteosarcoma increases the risk of side effects when using an increased dose of chemotherapy drug. Therefore, these factors limit the effectiveness of current treatments [1, 2]. Therefore, the use of heat as a localized treatment for cancer cells not only reduces drug resistance but also reduces side effects and damage to healthy tissues [3]. The idea of using heat for cancer treatment has been considered for a long time, but efforts have led to

* *Corresponding authors: Emails: hosseinimotlagh@meybod.ac.ir; f.oroojalian@ut.ac.ir; oroojalian.f@gmail.com*
Note. This manuscript was submitted on July 28, 2023; approved on September 25, 2023

its implementation in recent years. The main reason for this delay is the ability to create the optimal temperature rise in the localized point, so as not to damage the healthy cells and tissues of the body.

Thus, heat as a localized treatment for cancer cells reduces drug resistance and side effects in healthy tissues. Nowadays, different sources of heat have achieved this goal, like radio frequency [4], laser [5-8], and ultrasound [9].

The use of electromagnetic radiation to treat cancer has raised many hopes. However the main problem with using lasers is that they are non-selective, and their healthy and cancerous tissue is damaged in the radiation path; additionally, high power density is needed to destroy tumors [10]. To overcome these problems, the group of nanoparticles has entered this field and made the selectivity photo thermal method possible at lower powers and less time of radiation with higher efficiency [8, 11].

Ultrasound is also longitudinal waves with a frequency of more than 20 kHz that require a material environment to propagate [12]. As research shows, these mechanical waves have thermal and cavitation effects on cancerous tissues and can be used in the treatment of cancers such as prostate, pancreas, and breast [2, 9, 12, 13]. With the propagation of ultrasound waves, contraction and expansion areas are created in the tissue, so the local areas experience an alternative increase and decreased pressure. So, the gas bubble is formed and enlarged, called cavitation [14]. Then, as the ultrasonic wave cycles enhance, the volume of the drop increases and collapses. So, bubble energy released into the tissue environment increases the temperature, and tissue is thermally damaged [15]. Since cavitation is performed at high intensities, and ultrasonic waves at high intensities can damage healthy tissues [16], nanoparticles in the environment can create centers for cavitation bubbles. Thus, the intensity threshold of the cavitation waves is reduced, and healthy tissues are protected from the destructive effects of ultrasound at high intensities.

Of all the thermal therapeutic nano agents, graphene oxide (GO) has attracted much attention due to its unique properties. It has been considered due to its excellent mechanical, electrical, thermal, and optical properties, high surface area, and the possibility of controlling all these properties through chemical functionalization [16-20].

The first success in using carbon nanoparticles for photothermal treatment was achieved by Liu et al. in 2010 *in vivo* with intravenous injection and application of GO-PEGylated [21]. They found that PEGylated nano sheets effectively treated photo thermal in mice irradiated with near-infrared (NIR) wavelength at laser power 2 W/cm^2. Dia's research in 2011 is another example of photothermal therapy based on reduced GO sheets with high absorption at NIR [22]. A group in Italy used a pulse laser at 808 nm as a phase switch to control the release of drug-loaded on GO *in vivo* in 2014 [23]. They examined the release rate of DOX by changing various laser parameters, including pulse rate, flux, and spot size. Also, the impact of laser power and irradiation time in the NIR range and nanoparticle concentration GO were investigated to study chemo-photo thermal therapy of breast cancer in 2020 [5]. This study showed that the method of photothermal treatment has a higher efficiency than chemotherapy. Jane et al. investigated the effect of ultrasound on superficial tumors; also, they reported that ultrasound could increase the temperature of tumors and provide the conditions for their destruction in 1982 [24]. Gelet et al. found that high-intensity ultrasound was an effective treatment for prostate cancer in 1999 [25]. Also, Kaczmarek showed that using magnetic nanoparticles with ultrasound waves increased the yield of thermal therapy in 2018 [26]. The GO sonosensitizing effect and its comparison with gold and iron oxide nanoparticles were first analyzed by Beik et al. in 2016 [27]. They showed that gold nanoparticles are more potent Sonosensitizer agents than GO, and GO is stronger than iron oxide nanoparticles [28]. Also, Chen et al. synthesized a hybrid transonic base on reduced GO to SDT/hyperthermia cancer treatment under the low-power focus ultrasound condition [29].

As mentioned, separate studies have been performed on the thermal effects of lasers and ultrasounds in the presence of graphene oxide. So, in this study, researchers, for the first time, tried to investigate the thermal effect of laser at 808 nm and ultrasonic wavelengths on GO nanoparticles at the same condition and then compare them with each other. Also, the best result is used for the thermal treatment of MG63 cells. According to this, the thermal effect of laser and ultrasound devices is investigated in various powers and times of radiation at different concentrations of GO. Then, their therapeutic effect on osteosarcoma cancer is analyzed by the MTT test.

MATERIALS AND METHODS

GrapheneX supplied GO with 0.7-1.4 nm thickness and lateral size of approximately 5-100 µm (mean size

35 µm). Ethanol (493511, C_2H_5OH, molecular weight of 46.07 g⁄mol), HCL 37% (320331), Polyethylene glycol bis amine (PEG,14502), 3-[4,5-dimethylthiazol-2-yl]-2,5-dipheny-ltetrazolium bromide (MTT, M5655) were provided by Merck and N-[3- dimethylamino propyl-N0-ethylcar-bodiimide] hydrochloride (EDC, 03449) by Sigma Co.

A Jenway 6715 spectrophotometer was employed to record UV-Vis spectra ranging from 190-900 nm with 0.4 nm resolution. A 2 W- CW GaAs laser OEMDL-808[FC] by OElabs, was selected with good stability to carry out the laser exposure on the samples. Also, a bath sonicator (ELMASONIC S30H) and probsonicator (ChromTech-Taiwan) were exploited to investigate the sonodynamic effect.

GO PEGyltion

Briefly, the PEGylating of GO was performed by adding 72 mg of NaOH into GO and sonicating for 4 hours. Then, after adding HCl and removing the salts, PEG and EDC were injected into the solution. Next, another EDC was recharged to the solution and was stirred overnight at room temperature. Finally, it was centrifuged for removing any aggregates [5].

Characterization of GO

Zeta potential was evaluated by Brookhaven Corp Instruments (Holtsville, NY). Also, the images were captured by scanning electron microscopy (model EM3200, KYKY, China). For this purpose, the sample was coated with a gold layer after creating a thin film layer on the glass plate. Also, for preparing the sample for AFM, a drop of suspension was put on the mica surface and incubated for 5 minutes after making a suspension in ethanol or water. Then, the drop was removed by an airflow. Also, preparation of the sample for FTIR analysis was performed by the KBr plates.

Cell culture and statistical analysis

The cell line of MG63 cancerous was taken from Pasteur Institute (Tehran, Iran). Standard conditions for culturing these cells included DMEM medium (Gibco, Grand Island), 10% FBS (fetal bovine serum) (Gibco Grand Island), penicillin–streptomycin (Gibco, Grand Island) under 37˚C and 5% CO_2. *In vitro* evaluation of cellular uptake was performed according to reference [30, 31].

Also, the experiments were repeated 5 times for each data point and all data were statistically significant (*P*-value <= 0.05).

RESULT AND DISCUSSION

Characteristics of GO and GO-PEG

Fig. 1a shows FTIR spectra of GO and GO-PEG in the presence of peaks at 3447, 1632, and 1450 Cm^{-1} due to OH, C=O, and C=C vibrational bands, respectively. In addition, the bands at 3507 cm^{-1} are revealed due to N-H stretched GO-PEG vibrations [32]. Fig. 1b shows the properties of GO and GO-PEG.

Vis-UV spectra of GO have three peaks at 230,

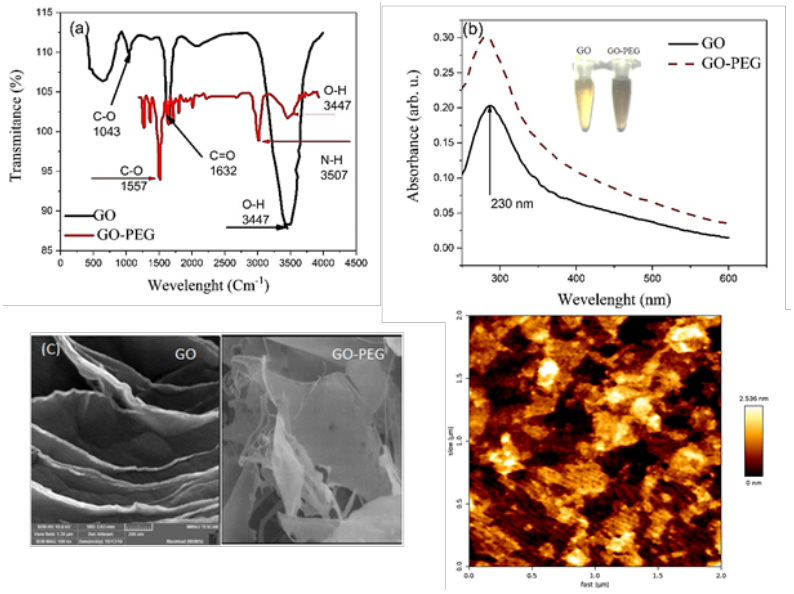

Fig. 1. (a) FTIR of GO and GO-PEG. The peak at 3507 cm^{-1} due to N-H vibrational bands confirms the binding of PEG to GO. (b) UV-Vis absorption spectra of GO and GO-PEG show increasing GO-PEG absorption versus GO. (c) SEM image of GO depicts the sheets of this nanoparticle and the presence of PEG on the PEGylated GO sheets. (d) AFM image of interest nanoparticles

300, and 364 nm; the strongest one appears at 236 nm and is usually due to the transition π → π* from the aromatic planer network of GO, While the peak of 300 nm shows the transition n → π* [33]. However, the peak of 364 nm represents the fine dispersion of the sheets and usually does not appear easily [34]. Fig. 1b also displays that GO absorption is increased at all wavelengths after PEGylation, which is apparent by changing the color of the GO-PEG from brown to darker.

SEM images of GO and GO-PEG in Fig. 1c shows that the presence of polymer on the GO surface according to PEGylation can separate the sheets, decrease the thickness, and increase the stability of nanoparticles in water.

Fig. 1d presents an AFM image of GO nanoparticles. According to it, the lateral size of GO nanoparticles is about 4.0 µm, and its thickness is about 3 nm. Since the thickness of each GO sheet is about 0.2-1 nm [35], this thickness indicates that each GO nanoparticle contains 3-10 sheets.

Fig. 2 Presents the zeta potential of GO and GO-PEG at pH=4.5. The Zeta potential of the GO peak is about -75 MV. GO-PEG Zeta potential exhibits to be more positive than GO due to the presence of amine groups at the edges of GO-PEG sheets.

Also, for selecting suitable concentrations of nanoparticles, the toxicity of GO-PEG was analyzed on MG63 cells by MTT test. Fig. 3 shows that PEGylated-GO represents less than 20% toxicity to low-concentration MG63 cells. Therefore, 2.0 and 4.0 mg/ml concentrations of GO-PEG were selected for the subsequent experiments due to their lower toxicity.

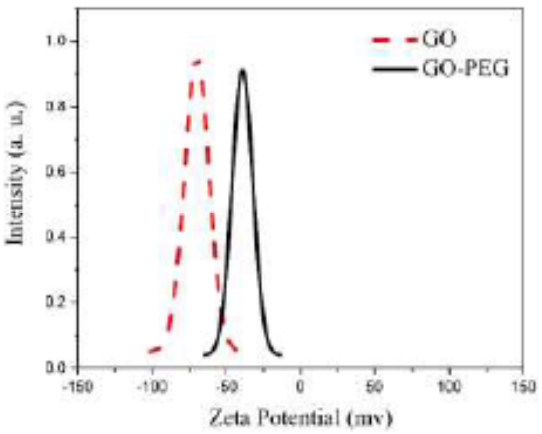

Fig. 2. Zeta potential of two components. It shows that the zeta potential is more positive due to the bonding of amine groups at PEG-GO

The effect of bath sonicator and heater

The effects of bath sonicate and heater on the temperature variations of GO-PEG and its surrounding water bath were investigated to compare the ultrasound effects (Fig. 4).

For this purpose, a microtube containing one milliliter of GO was placed in a glass vial filled with deionized water. The sample was warmed up with a heater, recorded the temperature of GO-PEG, and deionized for 10 min.

According to Fig. 5a, the temperature of GO-PEG and deionized water increases within 10 min, but the rate of temperature rise of deionized water is greater than GO-PEG. Over time, the rate of temperature rise of both samples decreases, which is depicted in Fig. 5a by elevating the graph's slope. But this slope reduction is slighter for deionized water. Therefore, the temperature of both samples is close to each other after 10 min.

Since the heat flux is from the heater to the deionized water, GO-PEG inside the microtube reaches it through heat conduction and causes its temperature to rise. As a result, in the beginning, the temperature of GO-PEG is significantly lower

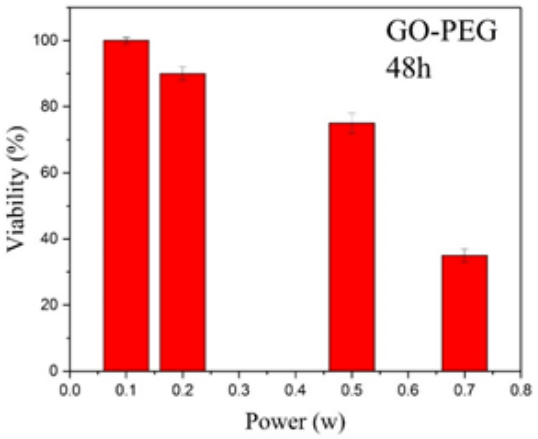

Fig. 3. Viability of MG63 cells versus Go-PEG concentration (0.1-0.7 mg/ml) for 48 hr

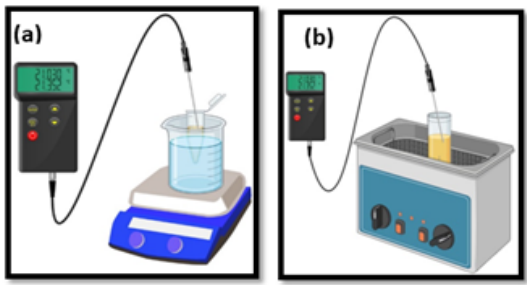

Fig. 4. Heating the GO-PEG solution by (a) heater and (b) bath sonicate

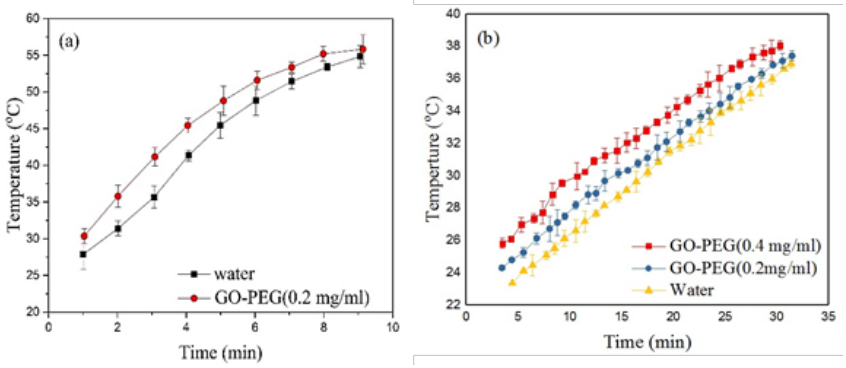

Fig. 5 The temperature rise of GO-PEG in various concentrations of 0.2 and 0.4 mg/ml and deionized water by (a) heater and (b) bath sonicate. The graph slopes are almost linear, and the temperature of the GO-PEG is close to deionized water over time

than the temperature of the deionized water because of this heat flux and the microtube wall. However, this temperature difference decreases during that time insofar as the temperature of the water and GO-PEG are almost equal.

Also, to analyze the effect of bath sonicate, 1 ml of GO-PEG in 0.2 and 0.4 mg/ml concentrations and 1 ml of deionized water were placed separately in a bath sonicate simultaneously for 30 minutes. The temperature variation between them was measured (Fig. 5b). According to Fig. 5b, the water temperature and the temperature of typical GO-PEG i. e. (0.2 and 0.44 mg/ml), increase linearly under 0-10 min. Also, the temperature rise of typical GO-PEG concentrations is higher than in deionized water. It is worth noting that Fig. 5b shows a temperature rise in terms of the concentration of GO-PEG, too. This phenomenon can be related to the increasing number of GO thermal conductive layers. Overall, there is an insignificant difference between increasing the temperature of the GO-PEG and water.

The effect of ultrasound

Like before, 1 ml of GO-PEG in 0.2 and 0.4 mg/ml concentrations and 1 ml of deionized water was ready for irradiation with ultrasound waves (Fig. 6a) at a power range of 2-3.5 W under 0-10 min. Fig. 7a-c depicts the temperature rise of GO-PEG and deionized water in terms of the exposure time at various ultrasound powers. In general, the temperatures of the samples increase in terms of concentration, exposure time, and ultrasound power exponentially (in contrast to the linear increase in temperature of the samples with bath sonicate and heater). Also, the graphs in all three samples get almost smooth after ten minutes. It must be mentioned that the temperature rise of the typical samples is not significantly different, and the presence of GO-PEG nanoparticles has not considerably increased the thermal effect of ultrasound, as shown in Fig. 7d.

In fact, the effect of ultrasonic waves at 2.3, 2.5, and 2.7 W power on temperature changes of deionized water and GO-PEG (0.2 mg/ml) have been almost the same, which can be attributed to various factors such as the distribution of nanoparticles, power, cavitation, hydrogen bonding obtained from the active groups of GO surface.

These results confirm the study of Beck In 2016 [27], which showed that GO at a concentration of 0.25 mg/ml irradiated by ultrasound waves at 1 W power can increase the temperature to only 2 °C and has less effect than gold nanoparticles.

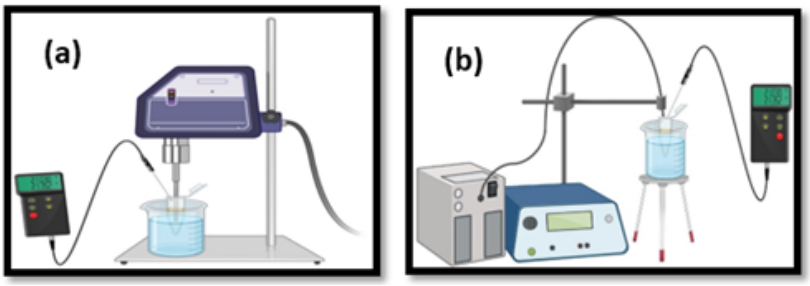

Fig. 6. Heating the GO-PEG solution by (a) probe sonicate and (b) laser.

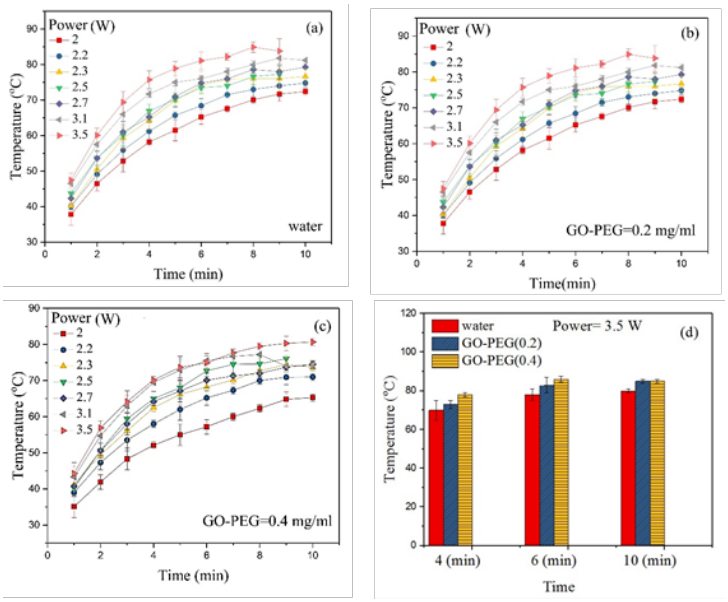

Fig. 7. Temperature rise of (a) deionized water and GO-PEG nanoparticles at concentrations (b) 0.2 and (c) 0.4 mg/ml varying at 2-3.3 w ultrasound power during time 10 min. (d) The comparison between temperature changes of these three samples in 4, 6, and 10 min at a max of power (3.5 W). It is evident that there is a significant temperature difference

Additionally, Shanei [14] investigated the synergistic effect of silver nanoparticles and 1MHz ultrasound on the rate of MCF-7 cell deaths. They reported that the silver nanoparticles can enhance the cytotoxicity of ultrasound waves and consequently increase cell death. Metal nanoparticles such as gold and silver are better converters than GO to convert ultrasound waves into heat.

The effect of laser radiation

The temperature rise of the GO-PEG and deionized water depends on concentrations of nanoparticles and laser properties such as average power and exposure time. Fig. 8a-c depicts the temperature rise of deionized water and GO-PEG regarding the exposure time at various laser powers. Generally, GO-PEG does show a significant

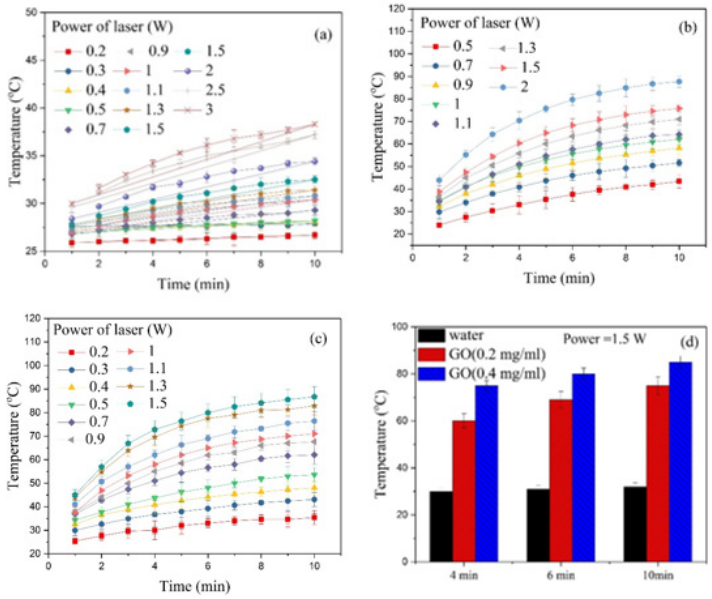

Fig. 8. Temperature variation of (a) water and GO-PEG at 0.2 (b) and 0.4 (c) mg/ml concentrations varying at 0.2-2 W laser power under 0-10 min. (d) comparing the temperate of water and interested GO-PEG concentration, i.e.. 0.2 and 0.4 mg/ml at 1.5 W for 4, 6, and 10 min

temperature rise in terms of concentration, laser power, and irradiation time in contrast to deionized water.

According to Fig. 8a, the diode laser at 808 nm raises the water temperature to less than 4˚C at 2 W under 10 min. This result confirms that a laser at 808 nm cannot significantly increase water temperature at a power of less than 2 W.

Fig. 8b and c depict that the temperature of GO-PEG increases higher than 50 °C. The GO-PEG concentration at 0.2 ml/mg was irradiated at 1 W after 5 min and at 0.4 ml/mg at 0.7 W after 3 min, which is the desired temperature for cancerous cell death.

Fig. 8d indicates that the laser cannot increase the water temperature to an acceptable level, and GO-PEG significantly affects the conversion of electromagnetic waves at 808 nm to heat. These results confirm our previous studies in the field of heat transfer by GO and laser [5].

Simulation and comparison of temperature between laser and ultrasound using a data mining approach

In each experiment, different factors affect the temperature of the solution. For instance, the GO concentration or radiation time can be used in different temperature values. However, investigating different parameters increases experimental time and cost. Simulation techniques can be used to build a computational model for measuring the effect of different values on the temperature to reduce cost and time. A regression tree is a famous data mining approach for simulation and predicting the most optimal situation [36, 37]. In this research, two regression trees are created to predict the Temperature values based on the amount of GO, Power, and Time of radiation of Laser and ultrasound. In the first regression tree, the model is created based on the effect of laser radiation. The overview of the three levels of the tree is depicted in Fig. 9. In the second tree, the effect of ultrasound is illustrated in Fig. 10. The regression tree is built on the training data points earned from the actual experiment. For example, “time=6 min, GO=0.2 mg/ml, power=0.9 W, and the temperature=51.5oC” is one of the data points for the laser experiment. In laser and Ultrasonic experiments, 248 and 160 sample data points are earned and used to build the trees consequently.

In each tree node, a parameter is checked, and based on its value, a child node (left or right node) is selected. Each path from the root node to the leaf nodes can predict the temperature value. For example, the path indicated by dashed arrows in Fig. 9 shows: “if (GO>0.1 mg/ml) and (power <=0.8 W) and (time <5.5 min) then the temperature is predicted as 35.857 with Mean Square Error (MSE)=40.486”.

The nodes of a regression tree are chosen to look for the optimum orders of parameters. For that purpose, different criteria exist. Gini and Entropy are two famous criteria for building trees. The critical parameters appear on the top of the tree using these criteria. For instance, in the laser tree, the concentration of GO is the most critical parameter because it is checked at the root node, and in the ultrasound tree, the radiation time is most important. Note that the GO concentration does not appear in the ultrasound tree, which means this parameter is not essential

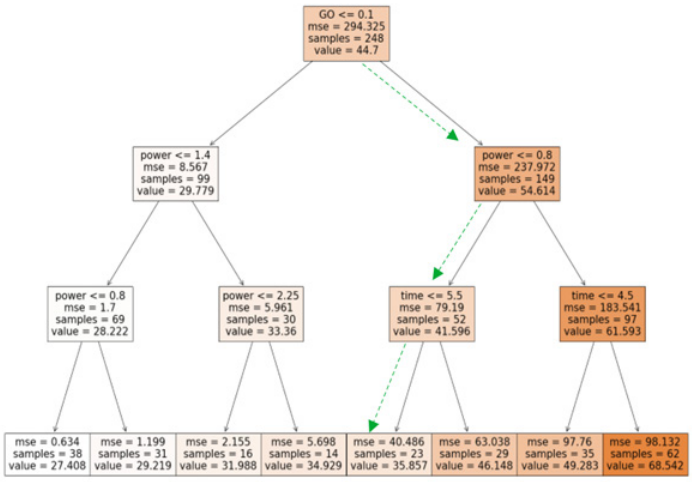

Fig. 9. Regression tree with three levels for simulating temperate under laser radiation. The GO parameter appears in the tree’s root, which shows GO is essential in predicting temperate.

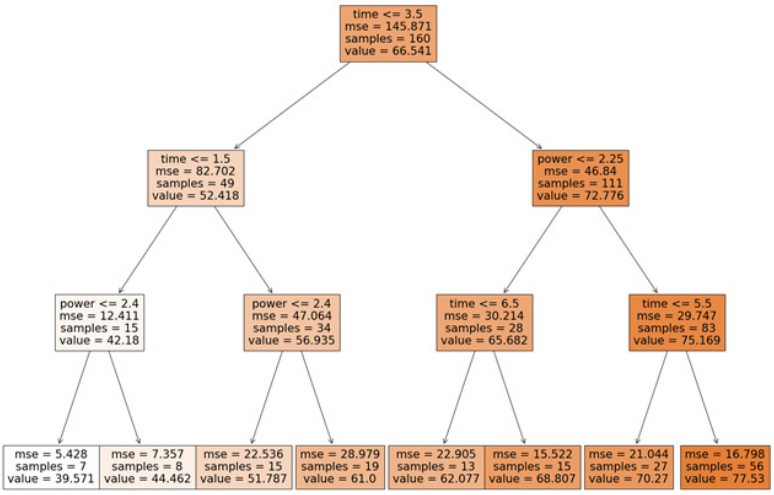

Fig. 10. Regression tree with three levels for simulating temperate under Ultrasonic radiation. The time parameter appears in the tree's root, which shows time is an important factor in predicting temperature

for temperature prediction.

Although GO nanoparticles did not play an influential role in converting ultrasound waves into heat, the results of this section show that this nanoparticle is a great photothermal nanoparticle and can convert infrared waves into heat as well. This feature can be completely effective in the photothermal therapy of cancer cells with fewer side effects. Therefore, the impact of laser and GO-PEG nanoparticles on Osteosarcoma cancer cell (MG63) death was investigated to confirm the laboratory results.

Simultaneous effect of laser and GO nanoparticles on cancerous cells

Notably, the wavelength at 808 nm is within the therapeutic window [6], and is expected not to heat and damage the cells effectively. This is confirmed by irradiating MG63 cells under laser exposure times 3, 6, and 10 min at various powers 0.75, 1.5, and 2 W. Fig. 11 illustrates the cell viability in terms of laser irradiation emphasizing slight cell mortality, especially at a laser power of less than 2 W and the cell viability is more than 90%. This result shows that a laser at 808 nm is suitable for penetrating cancerous tissue without damaging surrounding healthy cells. The final step is the simultaneous effect of nanoparticles and laser on the mortality of MG63 cancerous cells. Laser power at 0.7 and 1 W and irradiation time of 5 and 10 min are selected for investigating the photothermal effect of laser and GO-PEG.

Fig. 12 shows the cell viability for various concentrations of GO-PEG (0.2 and 0.4 mg/ml) under laser exposure at multiple powers. The cells undergo a notable reduction of viability of ~ 46%

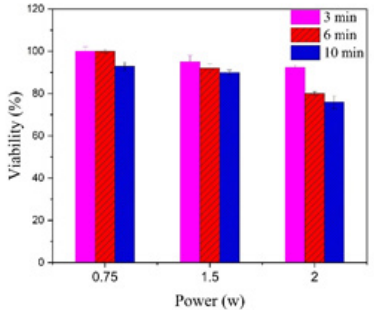

Fig. 11. Cell viability under laser irradiation at 0.73, 1.5, and 2 W on MG63 cells. As it is evident, the laser at less than 2 W power cannot damage the cell

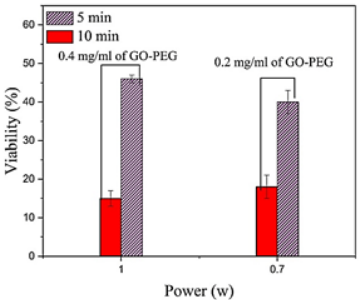

Fig. 12. *In vitro* synergistic effect of laser-treated GO-PEG on MG63 cells for two GO-PEG concentrations (0.2 and 0.4 mg/ml) at 0.7 and 1 W. Irradiation time is 5 and 10 min

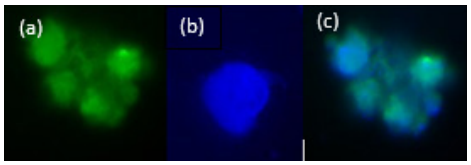

Fig. 13. Cellular uptake image of MG63 (a) GO-PEG-DIAL (b) Dapi and (c) merge of a and b

after 5 min and 15% after 10 min exposure time at power 1 W. Also, for the power of 0.7 W, viability is 40% after 5 min and 18% after 10 min. These results emphasize that increasing radiation time can lead to better cell death.

Also, Fig. 13 illustrates the uptake of GO-PEG after 24 hr by a fluorescent microscope so that the nanoparticles were stained with Dial and the cell with DAPI. Fig.13a-c shows the fluorescent image of GO, the nucleus of cells, and the presence of nanoparticles around the nucleus, respectively, which confirm the successful penetration of nanoparticles into the cells.

CONCLUSION

In this paper, we investigated the synergistic effect of GO-PEG nanoparticles with ultrasound and laser waves at 808 nm for the thermal treatment of osteosarcoma cancer cells (MG63). At first, the thermal effect of the heater and bath sonicate was studied on deionized water and GO-PEG.

The results show that the temperature increases linearly in the two environments. Additionally, the temperature of water and GO-PEG have a slight difference of about 1 ° C; over time, both temperatures converge.

Ultrasound waves of probe sonicate can raise water and GO-PEG temperature. Unlike the heater and sonicate, this increase is exponential and depends on the GO–PEG concentration, emphasizing the more GO-PEG concentration increases the temperature at a specific power and time. It is worth noting that the effect of GO-PEG on expanding the solution temperature is negligible compared to deionized water, and the increasing concentration of this nanoparticle can only increase the temperature by almost 3 or 4o C. It seems that GO-PEG is not a good absorber for ultrasound waves, and their conversion to heat that data mining simulation confirms it. The other form of GO may make the GO a better convertor for ultrasound waves.

To investigate the interaction of laser and GO-PEG, deionized water, and typical concentration of GO-PEG i. e. 0.2 and 0.4 mg/ml were irradiated by a continuous diode laser at 808 nm for 10 min with different powers of 0.1 - 2 W. The results showed that GO-PEG is a good photothermal agent for wavelength at 808 nm, unlike the ultrasound wave, while the temperature rise is exponential. Using GO photoexcitation increases the temperature above 60 °C, which is desirable for thermal therapy. Finally, the photothermal effect of GO was assessed on osteosarcoma (MG63) cells, which indicates cell mortality of more than 85%.

The preliminary results reported here suggest using the other form of GO or other nanoparticles to enhance the ultrasound effect. In comparison, GO is an excellent photothermal nanoparticle for localized thermal therapy of osteosarcoma cancer cells by laser at 808 nm with low side effects.

ACKNOWLEDGMENTS

The authors thank the nanostructured coating institute of Payame Noor University for using its lab.

FUNDING STATEMENT

The result of this study was extracted from a MSc thesis that was supported by Taft Payame Noor University (Grant No. 30231359).

DATA AVAILABILITY

The data are not publicly available due to governmental policy and privacy.

CONFLICTS OF INTEREST

The authors declare that there is no conflict of interest regarding the publication of this article.

REFERENCES

1. Litman T, Druley TE, Stein WD, Bates SE. From MDR to MXR: new understanding of multidrug resistance systems, their properties and clinical significance. Cell Mol Life Sci. 2001;58(7):931-959.
2. Sadeghi M, Kashanian S, Naghib SM, Askari E, Haghiralsadat F, Tofighi D. A highly sensitive nanobiosensor based on aptamer-conjugated graphene-decorated rhodium nanoparticles for detection of HER2-positive circulating tumor cells. Nano Rev. 2022;11(1):793-810.
3. Pourpirali R, Mahmoudnezhad A, Oroojalian F, Zarghami N, Pilehvar Y. Prolonged proliferation and delayed senescence of the adipose-derived stem cells grown on the electrospun composite nanofiber co-encapsulated with TiO2 nanoparticles and metformin-loaded mesoporous silica nanoparticles. Int J Pharm. 2021;604:120733.
4. Varon LAB, Orlande HRB, Eliçabe GE. Combined parameter and state estimation problem in a complex domain: RF hyperthermia treatment using nanoparticles. J Phys Conf Ser. 2016;745(3):032014.
5. Motlagh NSH, Parvin P, Mirzaie ZH, Karimi R, Sanderson JH, Atyabi F. Synergistic performance of triggered drug release and photothermal therapy of MCF7 cells based on laser activated PEGylated GO + DOX. Biomed Opt Express. 2020;11(7):3783-3794.
6. You J, Zhang R, Xiong C, Zhong M, Melancon M, Gupta S, et al. Effective photothermal chemotherapy using doxorubicin-loaded gold nanospheres that target EphB4 receptors in tumors. Cancer Res. 2012;72(18):4777-4786.
7. Wu H, Lu C, Chen M. Evaluation of minimally invasive laser ablation in children with osteoid osteoma. Oncol Lett.

2017;13(1):155-158.
8. Rashidi A, Omidi M, Choolaei M, Nazarzadeh M, Yadegari A, Haghierosadat F, et al. Electromechanical properties of vertically aligned carbon nanotube. Adv Mater Res. 2013;705:332-346.
9. Wood AK, Sehgal CM. A review of low-intensity ultrasound for cancer therapy. Ultrasound Med Biol. 2015;41(4):905-928.
10. Tu X, Ma Y, Cao Y, Huang J, Zhang M, Zhang Z. PEGylated carbon nanoparticles for efficient *in vitro* photothermal cancer therapy. J Mater Chem B. 2014;2(15):2184-2192.
11. Abdollahiyan P, Oroojalian F, Hejazi M, de la Guardia M, Mokhtarzadeh A. Nanotechnology, and scaffold implantation for the effective repair of injured organs: An overview on hard tissue engineering. J Control Release. 2021;333: 391-417.
12. Miller DL, Smith NB, Bailey MR, Czarnota GJ, Hynynen K, Makin IR. Overview of therapeutic ultrasound applications and safety considerations. J Ultrasound Med. 2012;31(4):623-634.
13. Yoshizawa S, Takagi R, Umemura S-i. Enhancement of High-Intensity Focused Ultrasound Heating by Short-Pulse Generated Cavitation. Appl Sci. 2017;7(3):288.
14. Shanei A, Tavakoli MB, Salehi H, Ebrahimi-Fard A. Evaluating the effects of ultrasound waves on MCF-7 cells in the presence of ag nanoparticles. J Isfahan Med Sch. 2016;34(389):763-768.
15. Legay M, Gondrexon N, Le Person S, Boldo P, Bontemps A. Enhancement of heat transfer by ultrasound: review and recent advances. Int J Chem Eng. 2011;2011:670108.
16. Li JL, Hou XL, Bao HC, Sun L, Tang B, Wang JF, et al. Graphene oxide nanoparticles for enhanced photothermal cancer cell therapy under the irradiation of a femtosecond laser beam. J Biomed Mater Res A. 2014;102(7):2181-2188.
17. Johari P, Shenoy VB. Modulating Optical Properties of Graphene Oxide: Role of Prominent Functional Groups. ACS Nano. 2011;5(9):7640-7647.
18. Omidi M, Malakoutian M, Choolaei M, Oroojalian F, Haghiralsadat F, Yazdian F. A Label-Free detection of biomolecules using micromechanical biosensors. Chin Phys Lett. 2013;30(6):068701.
19. Karimi MA, Dadmehr M, Hosseini M, Korouzhdehi B, Oroojalian F. Sensitive detection of methylated DNA and methyltransferase activity based on the lighting up of FAM-labeled DNA quenched fluorescence by gold nanoparticles. RSC advances. 2019;9(21):12063-12069.
20. Yaghoubi F, Naghib SM, Motlagh NSH, Haghiralsadat F, Jaliani HZ, Tofighi D, et al. Multiresponsive carboxylated graphene oxide-grafted aptamer as a multifunctional nanocarrier for targeted delivery of chemotherapeutics and bioactive compounds in cancer therapy. Nano Rev. 2021;10(1):1838-1852.
21. Yang K, Zhang S, Zhang G, Sun X, Lee S-T, Liu Z. Graphene in mice: Ultrahigh *in vivo* tumor uptake and efficient photothermal therapy. Nano Lett. 2010;10(9):3318-3323.
22. Robinson JT, Tabakman SM, Liang Y, Wang H, Sanchez Casalongue H, Vinh D, et al. Ultrasmall Reduced Graphene Oxide with High Near-Infrared Absorbance for Photothermal Therapy. J Am Chem Soc. 2011;133(17):6825-6831.
23. Matteini P, Tatini F, Cavigli L, Ottaviano S, Ghini G, Pini R. Graphene as a photothermal switch for controlled drug release. Nanoscale. 2014;6(14):7947-7953.
24. Marchal C, Bey P, Metz R, Gaulard ML, Robert J. Treatment of superficial human cancerous nodules by local ultrasound hyperthermia. Br J Cancer Suppl. 1982;5:243-245.
25. Gelet A, Chapelon JY, Bouvier R, Pangaud C, Lasne Y. Local control of prostate cancer by transrectal high intensity focused ultrasound therapy: preliminary results. J Urol. 1999;161(1):156-162.
26. Kaczmarek K, Hornowski T, Dobosz B, Józefczak A. Influence of Magnetic Nanoparticles on the Focused Ultrasound Hyperthermia. Materials (Basel). 2018;11(9). Epub 20180904.
27. Beik J, Abed Z, Shakeri-Zadeh A, Nourbakhsh M, Shiran MB. Evaluation of the sonosensitizing properties of nano-graphene oxide in comparison with iron oxide and gold nanoparticles. Phys E: Low-Dimens Syst Nanostructures. 2016;81:308-314.
28. Rahimizadeh M, Eshghi H, Shiri A, Ghadamyari Z, Matin MM, Oroojalian F, et al. Fe (HSO 4) 3 as an efficient catalyst for diazotization and diazo coupling reactions. J Korean Chem Soc. 2012;56(6):716-719.
29. Chen Y-W, Liu T-Y, Chang P-H, Hsu P-H, Liu H-L, Lin H-C, et al. A theranostic nrGO@MSN-ION nanocarrier developed to enhance the combination effect of sonodynamic therapy and ultrasound hyperthermia for treating tumor. Nanoscale. 2016;8(25):12648-12657.
30. yaghoubi f, Hosseini Motlagh NS, moradi a, Haghiralsadat f. Carboxylated Graphene Oxide as a Nanocarrier for Drug Delivery of Quercetin as an Effective Anticancer Agent Iran Biomed J. 2022;26(4):324-329.
31. Nia AH, Behnam B, Taghavi S, Oroojalian F, Eshghi H, Shier WT, et al. Evaluation of chemical modification effects on DNA plasmid transfection efficiency of single-walled carbon nanotube–succinate–polyethylenimine conjugates as non-viral gene carriers. Med Chem Comm. 2017;8(2):364-375.
32. Liu Z, Robinson JT, Sun X, Dai H. PEGylated nanographene oxide for delivery of water-insoluble cancer drugs. J Am Chem Soc. 2008;130(33):10876-10877.
33. Shang J, Ma L, Li J, Ai W, Yu T, Gurzadyan GG. Femtosecond pump–probe spectroscopy of graphene oxide in water. J Phys D: Appl Physics. 2014;47(9):094008.
34. Liaros N, Aloukos P, Kolokithas-Ntoukas A, Bakandritsos A, Szabo T, Zboril R, et al. Nonlinear optical properties and broadband optical power limiting action of graphene oxide colloids. J Phys Chem C. 2013;117(13):6842-6850.
35. Schniepp HC, Li J-L, McAllister MJ, Sai H, Herrera-Alonso M, Adamson DH, et al. Functionalized Single Graphene Sheets Derived from Splitting Graphite Oxide. J Phys Chem B. 2006;110(17):8535-8539.
36. Fatemi Bushehri SMM, Zarchi MS. An expert model for self-care problems classification using probabilistic neural network and feature selection approach. Appl Soft Comput. 2019;82:105545.
37. Sordillo LA, Pu Y, Pratavieira S, Budansky Y, Alfano RR. Deep optical imaging of tissue using the second and third near-infrared spectral windows. J Biomed Opt. 2014;19(5):056004.